# Oxygen-Induced Symmetrization and Structural Coherency in Fe/MgO/Fe(001) Magnetic Tunnel Junctions

C. Tusche,[1] H. L. Meyerheim,[1] N. Jedrecy,[2] G. Renaud,[3] A. Ernst,[1] J. Henk,[1] P. Bruno,[1] and J. Kirschner[1]

[1]*Max-Planck-Institut für Mikrostrukturphysik, Weinberg 2, D-06120 Halle, Germany**

[2]*Institut des NanoSciences de Paris, Universitès Paris 6 et 7, et CNRS-UMR 7588, 4 place Jussieu, F-75252 Paris Cedex 05, France*

[3]*CEA-Grenoble, 17 rue des Martyrs, F-38054 Grenoble, France*

(Received 11 July 2005; published 18 October 2005)

We present x-ray diffraction experiments and multiple-scattering calculations on the structure and transport properties of a Fe/MgO/Fe(001) magnetic tunnel junction (MTJ). Coherent growth of the top Fe electrode on the MgO spacer is observed only for Fe deposition in ambient oxygen atmosphere leading to a coherent and symmetric MTJ structure characterized by FeO layers at both Fe/MgO interfaces. This goes in parallel with calculations indicating large positive tunnel magnetoresistance (TMR) values in such symmetric junctions. The results have important implications for achieving giant TMR values.

DOI: 10.1103/PhysRevLett.95.176101 PACS numbers: 68.35.Ct, 61.10.−i, 75.70.Ak

Coherent tunneling in single-crystal magnetic tunnel junctions (MTJ's), where a monocrystalline oxide barrier is sandwiched between ferromagnetic electrodes is the key property to achieve tunnel magnetoresistance (TMR) values large enough for future high-density device applications [1–3].

Large TMR values, defined as $(R_{AP} - R_P)/R_P$ in terms of the tunnel resistances for antiparallel (AP, $R_{AP}$) and parallel (P, $R_P$) magnetizations of the electrodes, are achieved if Bloch states of different symmetries decay at different rates in the barrier. In the Fe/MgO/Fe MTJ, tunneling in the P alignment is dominated by contributions near $\vec{k}_{\parallel} = 0$ through the slowly decaying $\Delta_1$ state in the MgO spacer, leading to a small $R_P$ [4]. This mechanism is not present for AP alignment, giving rise to a large $R_{AP}$. Consequently, TMR values up to several 1000% were predicted theoretically on the basis of model structures involving abrupt Fe-MgO interfaces [4,5].

Structural perfection across the interfaces is a prerequisite for coherent tunneling, and intense experimental and theoretical studies were carried out to prepare optimized junctions [4–10]. For the Fe/MgO/Fe(001) prototype system, TMR values up to 250% were achieved [9].

The decisive role of the atomic structure on the transport properties in Fe/MgO/Fe MTJ's was proven in recent studies on resonant tunneling through interface states involving minority-channel conductance [7] and by observation of an asymmetric current-voltage characteristic [6,8,9]. The latter was tentatively attributed to asymmetric interface structures. The assumption of different interface structures is doubly justified. First, the growth of Fe on MgO is different from MgO growth on Fe due to the different surface free energies of MgO (1.1 J/m$^2$) and Fe (2.9 J/m$^2$). Layer-by-layer growth is favored for MgO on Fe but not vice versa [11,12]. Second, experimental evidence by surface x-ray diffraction (SXRD) was given for an FeO interface layer between the Fe(001) bottom electrode and the MgO barrier [13]. Recent calculations have shown that the FeO interface layer reduces the TMR by reducing the coupling of the $\Delta_1$ state in the MgO spacer to the Fe electronic Bloch states [10].

Despite strong evidence for the key role played by the geometric structure on the TMR, no crystallographic analysis of a complete MTJ structure as well as its dependence on the preparation conditions has been carried out thus far. SXRD experiments measuring the intensity distribution along the integer order crystal truncation rods (CTR's) of the Fe(001) substrate not only probe the interface structure but are sensitive to the registry of subsequently deposited layers with respect to the substrate electrode. To this end we have applied SXRD to study differently prepared Fe/MgO/Fe(001) MTJ's.

The samples were prepared as follows: First, a two monolayer (ML) thick MgO film was deposited at a rate of $F = 0.125$ ML/min from a polycrystalline MgO rod heated by electron bombardment under ultrahigh vacuum (UHV) conditions (base pressure $10^{-10}$ mbar) on the clean Fe(001) single-crystal surface ($\varnothing = 7$ mm). This was followed by deposition ($F = 0.25$ ML/min) of an 8 ML thick Fe film using molecular beam epitaxy (here and in the following we define the coverage of 1 ML as one adatom per substrate atom, i.e., $1.21 \times 10^{15}$ atoms/cm$^2$).

For the top Fe layer deposition, two kinds of preparations were used. In the first, the upper Fe film was deposited under UHV conditions. In the second, Fe deposition was carried out under $10^{-7}$ mbar ambient oxygen pressure up to 0.5 ML coverage. At this point the oxygen exposure was stopped and Fe deposition was continued under UHV conditions. In the following we call the samples A for UHV deposition and B for oxygen-assisted deposition.

SXRD measurements were carried out *in situ* at the beam line BM32 of the European Synchrotron Radiation Facility (ESRF) using a UHV diffractometer. Integrated x-ray intensities were collected at grazing incidence of the

 

incoming beam ($\lambda = 0.68$ Å) along four symmetry independent [(10), (11), (20), and (21)] CTR's by rotating the sample about its surface normal [14]. The CTR's arise due to truncation of the crystal. Therefore, the reciprocal space coordinate ($\ell = q_z/c*$) along the surface normal is a continuous parameter [15]. The parameters $q_z$ and $c*$ represent the momentum transfer normal to the surface and the reciprocal lattice unit (rlu) of the iron crystal, respectively.

Figure 1 shows the structure factor amplitudes ($|F|$) measured up to $q_z = 2.3$ rlu, equivalent to $q_z = 3.53$ Å$^{-1}$. They were derived after correcting the integrated intensities for geometric factors [14]. Circles and triangles represent data points collected for samples A (upper curves) and B (lower curves), respectively. Standard deviations ($\sigma$) represented by error bars were derived from the counting statistics and the reproducibility of symmetry equivalent reflections [16]. In general, these were found to be in the 7% range.

As compared to the CTR's of sample A, those of sample B are considerably more structured. This directly shows that more layers contribute to the total scattering amplitude in the latter case. The quantitative analysis was carried out by least-squares refinement of the $|F|$'s calculated for a model structure to the measured ones. Because of the $p4mm$ site symmetry of the atomic positions within the surface unit cell [$(x, y)$ either at (0, 0) or (1/2, 1/2)] only the $z$ position and site occupancy needs to be varied in each layer. Complete Fe and MgO layers are described by one Fe as well as by one Mg and O atom within the surface unit cell, respectively. Occupancy factors less than 1.0 represent incomplete layers. In addition to the MgO and the top Fe electrode layers, also the two uppermost substrate Fe layers were included in the refinement. Taking account of deeper layers did not improve the fits.

Solid lines in Fig. 1 represent the best fits according to the structure models discussed below. Direct eye inspection indicates that all details of the experimental curves are almost perfectly reproduced. This is expressed by the unweighted residual ($R_u$) in the 5%–10% range, which for SXRD studies and the complexity of the samples is an excellent value [16].

Figure 2 compares the layer-resolved composition for samples A (a) and B (b). The lengths of the bars represent the concentrations of the different species Fe (dark gray or blue), Mg (light gray or yellow), and O (hatched areas) in each layer. The composition of each metal and oxide layer is given by the labels on the left (in brackets), where the subscripts indicate the fractional occupancy of the respective phases.

In agreement with previous results [13], for both samples a substoichiometric oxygen layer ($FeO_x$, $x \approx 0.5$–$0.6$) at the lower Fe/MgO interface is found (the error bar for the concentration determination is about 10%). MgO grows in a layer-by-layer mode on Fe(001). We

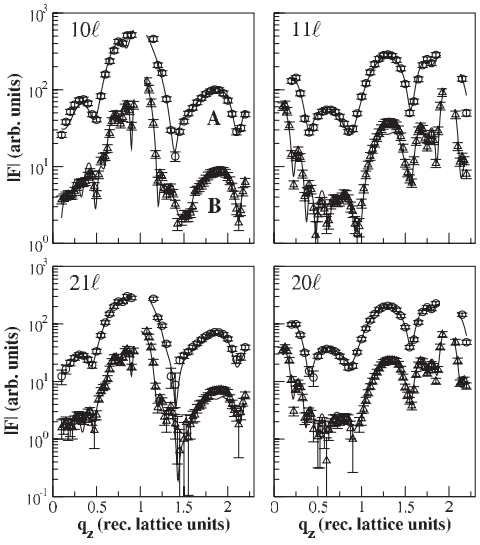


FIG. 1. Measured (symbols) and calculated (lines) distribution of the structure factor amplitude ($|F|$) along the (10), (11), (20), and (21) CTR's. Circles and triangles represent data collected for sample A (UHV deposition of top Fe electrode) and B (oxygen-assisted deposition), respectively. Curves are shifted vertically for clarity.

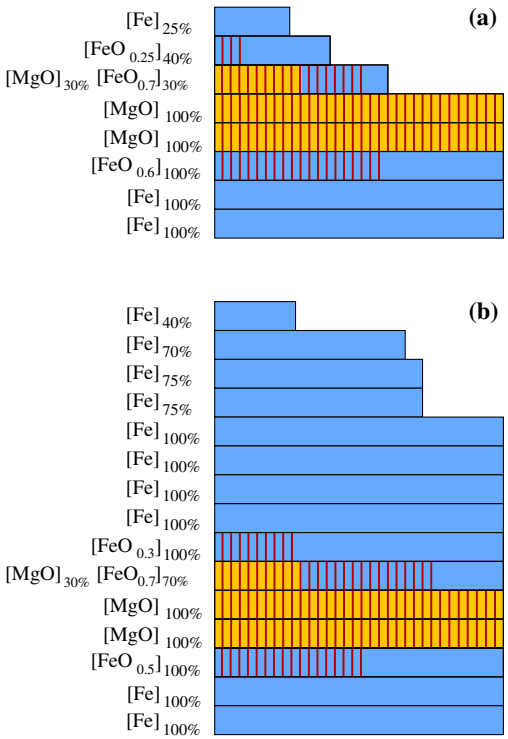


FIG. 2 (color online). Concentration profiles for sample A (a) and B (b) obtained by SXRD. Blue (dark gray) and yellow (light gray) bars represent Fe and Mg, respectively. Superimposed hatched areas represent oxygen. Labels on the left indicate the layer compositions, in which fractional occupancies in percent of a ML are given by subscripts to square brackets.

find a total coverage of 2.3 ML MgO for both samples due to some overdosing.

Significant differences between samples A and B exist for the subsequently grown parts of the MTJ. Most importantly, for sample A, although 7.8 ML were deposited as confirmed by Auger electron spectroscopy, only 0.95 ML Fe contribute to the SXRD signal. It is concluded that the remaining Fe (6.7 ML) is not in registry with the underlying crystal lattice. Additional evidence for disordered Fe comes from an increased background level in low energy electron diffraction patterns. In contrast, for sample B, all the deposited Fe contributes to the SXRD data, indicating a high degree of structural order throughout the whole MTJ. Layer-by layer growth is perfect for the first 5 Fe layers, but subsequently deposited layers are not complete, indicating a tendency to form three-dimensional islands [see Fig. 2(b)].

Coherent growth of the upper Fe electrode in B is attributed to the formation of an $FeO_x$ interface layer between the MgO spacer and the Fe layer. For sample A we find above the two complete MgO layers 30% of a ML of MgO (from overdosing) and only 30% of a ML of $FeO_x$ ($x \approx 0.7$). In contrast, for B $FeO_x$ fills this layer completely (70% of a ML).

It should be noted that even in the absence of oxygen supply (A) some Fe is oxidized at the interface. One may speculate that the amount of oxygen necessary for Fe oxidation comes from deposited MgO, but within an uncertainty of 10% there is no evidence for any deviation from the Mg:O = 1:1 stoichiometry throughout the layers. One possibility could be that upon Fe deposition MgO might be reduced, thereby "consuming" some parts of the MgO layer. Support for the relation between Fe oxidation and MgO comes from the observation that also a minor part of second layer Fe is oxidized as indicated by the labels $FeO_{0.25}$ in Fig. 2(a) and $FeO_{0.30}$ in Fig. 2(b), possibly by contact with the (overdosed) MgO islands in the layer beneath. Although the verification of this model requires further studies, in summary we have evidence that a partial oxidation of the top Fe electrode takes place also in the absence of oxygen supply.

In a thermodynamic description, layer-by-layer growth of Fe is understood in terms of an $FeO_x$ induced modification of the interface contribution to the free energy. The interface energy contains the specific chemical interaction between film and substrate. Introduction of the $FeO_x$ interface layer reduces the interface energy leading to complete wetting of the surface. For details we refer to Ref. [17].

A crystallographic view of the interface structure in sample B is shown in Fig. 3. Blue balls represent Fe atoms, and Mg and O atoms are represented by yellow and red balls, respectively. Interlayer distances given in Å are indicated on the left (error bar $\approx 0.05$ Å). Interfacial O atoms are randomly distributed within the $FeO_x$ layer, since no superstructure is observed. There is an enhanced

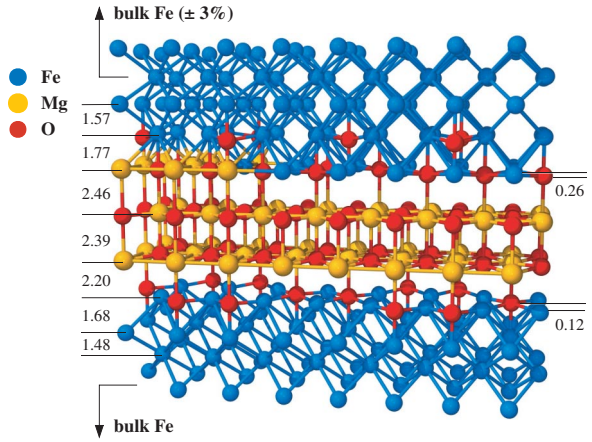


FIG. 3 (color). Model of the interface structure in sample B. Blue balls represent Fe atoms, and red and yellow balls O and Mg atoms, respectively. Distances are given in angstrom units.

interlayer spacing between the $FeO_x$ and the adjacent Fe layers (1.68 and 1.77 Å), corresponding to 18% and 23% expansion relative to the Fe bulk spacing (1.43 Å). Expansions are rapidly damped away from the interface and only the second interlayer distance is expanded (1.48 and 1.57 Å). There is some rumpling within the $FeO_x$ layers, where the O atoms are located 0.12 Å above (bottom interface) and 0.26 Å below (top interface) the Fe position. Because of the lateral 3.7% compression of the MgO layer to adapt to the Fe lattice (bulk lattice constant: 4.21 Å versus 4.05 Å for Fe), the MgO layers are tetragonally expanded; however, the determined value of 14% is larger than expected by continuum elasticity theory (2.5%), possibly due to the interaction with the $FeO_x$ interface.

Oxygen-assisted growth of a coherent MTJ is directly related to the presence of a symmetric interface characterized by *complete* and coherent $FeO_x$ layers. The lack of registry of the top Fe electrode in sample A has considerable impact on the propagation of the scattering channels (Bloch states) from the MgO spacer into the Fe electrode since coherent tunneling in which the parallel momentum ($\vec{k}_{\parallel}$) is conserved is less probable. This might explain significant differences between the TMR values derived from theory (always coherent structures) and the experimental ones.

Former theoretical studies for Fe/MgO/Fe indicated a strong sensitivity of the TMR on structural parameters. They show further that the conductance depends strongly on the symmetry of the involved electronic states (Bloch states in the electrodes and evanescent states in the barrier). Oxidation of one of the interface Fe layers leads to a considerable reduction of the conductances [10,18]. In the present theoretical investigation, we focus on effects of the symmetrization of Fe/MgO/Fe(001) interfaces on the TMR, with regard to the present experiment.

To study the impact of the MTJ structure on the TMR, first-principles Kohn-Korringa-Rostoker calculations of

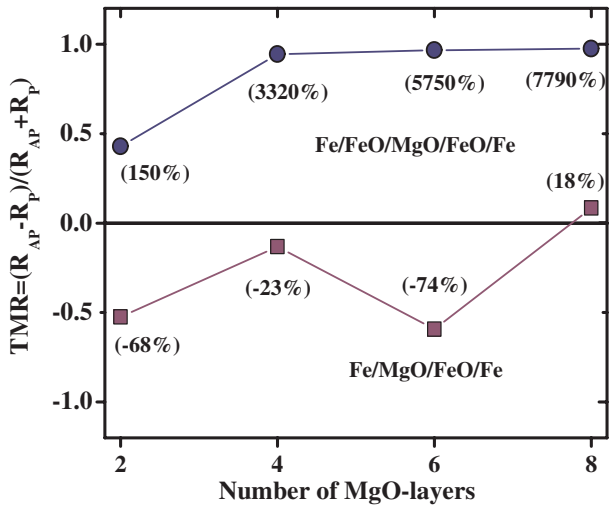


FIG. 4 (color online). Calculated normalized TMR values $[(R_{AP} - R_P)/(R_{AP} + R_{RP})]$ for symmetric Fe/FeO/MgO/FeO/Fe and asymmetric Fe/MgO/FeO/Fe MTJ vs MgO thickness. Values in brackets are defined by TMR $= (R_{AP} - R_P)/R_P$.

the electronic structure and of the conductance were performed. Calculations for all barrier configurations were performed self-consistently within the atomic sphere approximation, using the local spin-density approximation with the Perdew-Wang [19] exchange-correlation potential. The self-consistent potentials were subsequently used in the calculations of the ballistic conductance within Landauer-Büttiker theory [20], following the approach reported in Refs. [4,21]. Since the conductance is very sensitive to the $\vec{k}_{\|}$ integration, 40 000 $\vec{k}_{\|}$ points were used in the full two-dimensional Brillouin zone. According to scattering boundary conditions, semi-infinite Fe leads were taken.

Two model systems were assumed, which are characterized by one (Fe/FeO/MgO/Fe, asymmetric MTJ) and two (Fe/FeO/MgO/FeO/Fe, symmetric MTJ) FeO interfaces, respectively. The geometry was adopted from the experiment, but stoichiometric $FeO_x$ layers ($x = 1$) were assumed. Since the effect of the interface structure is expected to be larger for thin than for thick MgO barriers, their thickness was varied from 2 to 8 ML.

Figure 4 shows the normalized TMR for both model structures versus MgO spacer thickness. Values in brackets are TMR values according to the often used ''optimistic'' TMR definition (see introduction). The most striking result is that the sign of the TMR depends on the symmetry of the structure: the symmetric structure results in a large positive TMR, which increases with MgO thickness. In contrast, the TMR is negative for the asymmetric structures, a finding in agreement with recent work [10]. Its magnitude oscillates with increasing MgO thickness, and a small positive TMR is obtained for 8 ML MgO. The difference in behavior is explained by interface resonance states induced by the $FeO_x$ layer, which in the case of a symmetric MTJ are present on *both sides* of the spacer. This leads to a strong enhancement of the (P) conductance through these states (''hot spots''). Absence of one $FeO_x$ layer as in the asymmetric case reduces the density of states of the interface resonances and consequently results in less efficient tunneling.

In summary, we have presented a joint structural and theoretical study on the Fe/MgO/Fe(001) MTJ. The structure analysis indicates a strong dependence of the interface and layer composition on the deposition conditions. Oxygen-assisted symmetrization of the tunnel junction involving two FeO interface layers leads to a fully coherent MTJ, a prerequisite for giant TMR values required for technological applications.

We (C. T., H. L. M., and N. J.) thank Mrs. Noblet for her technical assistance and the ESRF for the hospitality during our visit. C. T. acknowledges support by the Forschergruppe 404 of the German Science Foundation (DFG).

*Electronic address: hmeyerhm@mpi-halle.mpg.de

[1] S. A. Wolf *et al.*, Science **294**, 1488 (2001).
[2] M. Bowen *et al.*, Appl. Phys. Lett. **79**, 1655 (2001).
[3] W. Wulfhekel *et al.*, Appl. Phys. Lett. **78**, 509 (2001).
[4] W. H. Butler, X.-G. Zhang, T. C. Schulthess, and J. M. MacLaren, Phys. Rev. B **63**, 054416 (2001).
[5] J. Mathon and A. Umerski, Phys. Rev. B **63**, 220403(R) (2001).
[6] J. Faure-Vincent *et al.*, Appl. Phys. Lett. **82**, 4507 (2003).
[7] C. Tiusan *et al.*, Phys. Rev. Lett. **93**, 106602 (2004).
[8] S. Yuasa, A. Fukushima, T. Nagahama, K. Ando, and Y. Suzuki, Jpn. J. Appl. Phys. **43**, L588 (2004).
[9] S. Yuasa, T. Nagahama, A. Fukushima, Y. Suzuki, and K. Ando, Nat. Mater. **3**, 868 (2004).
[10] X.-G. Zhang, W. H. Butler, and A. Bandyopadhyay, Phys. Rev. B **68**, 092402 (2003).
[11] L. Z. Mezey and J. Giber, Jpn. J. Appl. Phys. **21**, 1569 (1982).
[12] S. H. Overbury, P. A. Bertrand, and G. A. Somorjai, Chem. Rev. **75**, 547 (1975).
[13] H. L. Meyerheim *et al.*, Phys. Rev. Lett. **87**, 076102 (2001).
[14] E. Vlieg, J. Appl. Crystallogr. **30**, 532 (1997).
[15] I. K. Robinson, Phys. Rev. B **33**, 3830 (1986).
[16] I. K. Robinson and D. J. Tweet, Rep. Prog. Phys. **55**, 599 (1992).
[17] E. Bauer and J. H. van der Merwe, Phys. Rev. B **33**, 3657 (1986).
[18] D. Wortmann, G. Bihlmayer, and S. Blügel, J. Phys. Condens. Matter **16**, S5819 (2004).
[19] J. P. Perdew and Y. Wang, Phys. Rev. B **45**, 13 244 (1992).
[20] R. Landauer, IBM J. Res. Dev. **1**, 223 (1957).
[21] J. M. MacLaren, X.-G. Zhang, W. H. Butler, and Xindong Wang, Phys. Rev. B **59**, 5470 (1999).